JOURNAL OF GEOPHYSICAL RESEARCH, VOL. 102, NO. D25, PAGES 29,929–29,937, DECEMBER 27, 1997

Atmospheric Radiation Measurements Enhanced Shortwave Experiment (ARESE): Experimental and data details

Francisco P. J. Valero, Anthony Bucholtz, Brett C. Bush,
Shelly K. Pope, William D. Collins,[1] and Piotr Flatau
Atmospheric Research Laboratory, Center for Atmospheric Sciences, Scripps Institution of Oceanography, University of California, San Diego, La Jolla

Anthony Strawa and Warren J. Y. Gore
NASA Ames Research Center, Moffett Field, California

Abstract. Atmospheric Radiation Measurements Enhanced Shortwave Experiment (ARESE) was conducted to study the magnitude and spectral characteristics of the absorption of solar radiation by the clear and cloudy atmosphere. Three aircraft platforms, a Grob Egrett, a NASA ER-2, and a Twin Otter, were used during ARESE in conjunction with the Atmospheric Radiation Measurements (ARM) central and extended facilities in north central Oklahoma. The aircraft were coordinated to simultaneously measure solar irradiances in the total spectral broadband (0.224–3.91 μm), near infrared broadband (0.678–3.3 μm), and in seven narrow band-pass (~10 nm width) channels centered at 0.500, 0.862, 1.064, 1.249, 1.501, 1.651, and 1.750 μm. Instrumental calibration issues are discussed in some detail, in particular radiometric power, angular, and spectral responses. The data discussed in this paper are available at the ARM ARESE data archive via anonymous FTP to ftp.arm.gov.

1. Introduction

The amount of solar energy that reaches the top of the Earth's atmosphere has been measured with great accuracy. However, the distribution of this energy in the planetary system (atmosphere plus surface) is still one of the least quantified parameters required to understand and describe the climate system [*Kiehl and Tremberth*, 1997].

According to current theoretical understanding the absorption of solar radiation by an atmospheric column containing clouds is about equal to the absorption by the same column in the absence of clouds. In contrast, experimental investigations during the last several decades have shown that the observed magnitude of the absorption of solar radiation by the cloudy sky exceeds model predictions by varying amounts [*Stephens and Tsay*, 1990]. More recently, *Cess et al.* [1995], *Ramanathan et al.* [1995], *Pilewskie and Valero* [1995], *Li et al.* [1995], and *Waliser et al.* [1996] confirm the previous observational findings at tropical latitudes. *Kondratiev et al.* [1996] and *Chou and Zhou* [1997] also indicate that clouds absorb more solar radiation than predicted by theory. *Valero et al.* [this issue] and *Zender et al.* [this issue] report similar findings at midlatitudes over the North American continent.

Cess et al. [1995] used collocated satellite-surface measurements at four different locations (American Samoa, Barrow, Boulder, and Cape Grim) to evaluate the absorption of solar radiation by clouds. A comparison with the European Centre for Medium-Range Weather Forecasts (ECMWF) Model and Version 2 of the National Center for Atmospheric Research Community Climate Model (CCM2) shows that the observations and theoretical calculations differ by a substantial amount as discussed in the previous paragraph. *Pilewskie and Valero* [1995] made measurements of cloud absorption during the Tropical Ocean Global Atmosphere-Coupled Ocean Atmosphere Response Experiment (TOGA-COARE) and the Central Equatorial Pacific Experiment (CEPEX) using direct, simultaneous aircraft observations above and below clouds in major tropical cloud systems.

Studies by *Arking* [1996] and *Imre et al.* [1996] claim that it is enhanced clear-sky absorption that produces the measured absorption in excess of theory predictions. Other studies by *Stephens* [1996], *Li and Moreau* [1996], *Francis et al.* [1997], *Ackerman and Toon* [1996], and *King et al.* [1990] claim small or negligible excess absorption by clouds. *Stephens* [1996] and *Francis et al.* [1997] base their conclusions upon indirect estimates of the absorption by clouds; they compare modeled and measured cloud albedos and transmittance assuming, following the standard understanding, that any excess absorption must exclusively occur in the near-infrared spectral region where water absorption bands are known to exist. *Ackerman and Toon* [1996] use purely theoretical calculations also assuming that absorption by clouds occurs only in the near-infrared; *Li and Moreau* [1996] consider the possibility of aerosol effects; *King et al.* [1990] find, from observations within a marine stratocumulus cloud, comparatively small discrepancies between theory and spectral diffuse domain observations used to determine cloud single scattering albedo.

Attempts have been made to explain the difference between measurements and calculations by postulating that horizontal transport of photons by clouds results in an "apparent" absorption [*Ackerman and Cox*, 1981; *Stephens*, 1996]. Figure 1 illustrates schematically the possible case of a single, isolated

[1]Now at National Center for Atmospheric Research, Boulder, Colorado.

Copyright 1997 by the American Geophysical Union.

Paper number 97JD02434.
0148-0227/97/97JD-02434$09.00

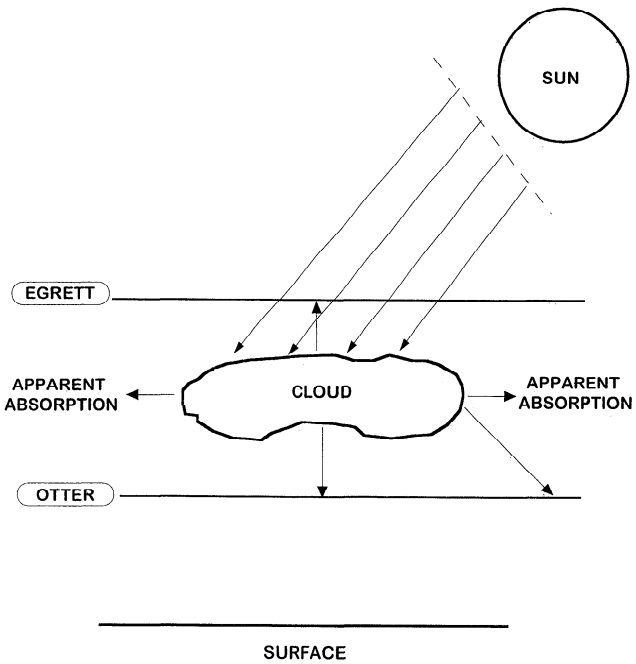

Figure 1. This sketch illustrates the idea that horizontal scattering of photons by clouds can result in an apparent absorption.

cloud, for which two fixed hemispherical field of view radiometers, located above and below the cloud, could miss photons scattered in nearly horizontal directions.

The uncertainties described above, along with the lack of a possible explanation or a definitive mechanism, led to the Atmospheric Radiation Measurements (ARM) Enhanced Shortwave Experiment (ARESE). The primary goals of ARESE were to obtain sets of measurements to determine accurately the absorption of solar radiation by the clear and cloudy atmospheric column at midlatitudes, to investigate the spectral regions where the excess absorption occurs, and to answer the question, Is the measured absorption real, or is it the result of "apparent absorption" resulting from the horizontal transport of photons by clouds? A secondary but fundamental goal was to begin the process of identifying the physical mechanism responsible for the absorption, or the inability of the models to reproduce the observations. In this paper, the experimental aspects of the research are summarized; a detailed analysis of the data is made in two other papers, *Zender et al.* [this issue] and *Valero et al.* [this issue].

2. Experiment

Following the previous discussion and to meet the goals described above, the experimental emphasis of ARESE involved the acquisition of radiometric data by multiple, coordinated aircraft and from surface sites. The aircraft covered the range from the lower stratosphere to the low troposphere. Surface observations were made from the ARM Clouds and Radiation Testbed (CART) central facility located at 97.48° longitude and 36.59° latitude and from secondary surface stations (extended facilities) which are part of the ARM Southern Great Plains (SGP) site.

The absorption by the atmospheric layer between two altitudes (the flux divergence) is defined as the difference between the net fluxes at each level in the atmosphere. The net radiative flux is the difference between the downwelling and upwelling fluxes at each altitude. Net solar flux must be acquired simultaneously at both flight altitudes to minimize the uncertainties associated with cloud advection, evolution, three-dimensional effects, etc. The net flux at a given altitude is the absorption by the column and the surface below.

The aircraft, stacked at different altitudes, flew tracks over the surface stations. In this manner, it was possible to obtain coeval measurements of radiative fluxes from which the absorption of radiation by the atmosphere was computed [*Valero et al.*, this issue]. Surface observations provided the radiative flux transmitted through the column.

Radiative flux measurements at the stratosphere, the upper troposphere, and the lower troposphere were made using the NASA ER-2, a Grob Egrett, and a Twin Otter aircraft, respectively. All three aircraft were equipped with identical radiometric instrumentation, as were the surface sites. Table 1 lists the dates, observational platforms, and atmospheric conditions encountered during the ARESE radiometric observations.

3. Instrumentation

The basic instruments, in addition to the CART site facilities, required to meet the ARESE objectives are included in the radiation measurement system (RAMS). The RAMS is a multiple array of radiometers covering the spectrum from the near-ultraviolet to the far (thermal) infrared. Components of the RAMS vary depending on the purpose and platform being used.

3.1. Aircraft

During ARESE the following aircraft radiometers, pointing in zenith and nadir directions, were utilized:

3.1.1. Twin Otter and Egrett. (1) Total Solar Broadband Radiometers (TSBR) covered the spectral range from 0.224 to 3.91 μm [*Valero et al.*, 1982]. (2) Fractional Solar Broadband Radiometers (FSBR) covered the near-infrared spectral range from 0.678 to 3.3 μm [*Valero et al.*, 1982]. (3) Total Direct Diffuse Radiometers (TDDR) covered seven spectral channels in the solar spectrum centered at 0.500, 0.862, 1.064, 1.249, 1.501, 1.651, and 1.750 μm with a band pass of about 10 nm [*Valero et al.*, 1989].

3.1.2. ER-2. The ER-2 was equipped with the RAMS, a camera, a lidar [*Spinhirne et al.*, 1996] and the Modis Airborne Simulator (MAS) [*King et al.*, 1996].

3.2. Surface

Zenith pointing RAMS instruments identical to those in the aircraft were installed at the CART central facility and the extended facilities at Byron and Ringwood in Oklahoma.

4. Radiometric Calibrations

The RAMS broadband radiometers use electrically calibrated pyroelectric detectors, which are by themselves absolute devices [*Geist and Blevin*, 1973; *Valero et al.*, 1982]. Each instrument is individually built, quality controlled, and characterized. Components of the electronic circuits of each radiometer are custom matched to the individual detector elements.

The RAMS broadband radiometers are very different from other commonly used instruments. For this reason, we will briefly describe their operational principles since they are im-

Table 1. ARESE Radiometric Observations

Day	Date	Aircraft	Ground Stations	Conditions
268	Sept. 25	ER-2, Egrett, Twin Otter		broken clouds
269	Sept. 26	ER-2		scattered clouds
270	Sept. 27	ER-2		(satellite calibration, Gulf of Mexico)
271	Sept. 28	ER-2		low clouds and cirrus
272	Sept. 29	ER-2, Egrett, Twin Otter		scattered clouds
276	Oct. 3	ER-2, Twin Otter		clear sky
279	Oct. 6	ER-2		(survey of hurricane-damaged areas)
284	Oct. 11	ER-2, Egrett, Twin Otter	L, R	clear sky
285	Oct. 12	ER-2		(satellite calibration, Gulf of Mexico)
286	Oct. 13	Egrett, Twin Otter	L, B	broken-to-solid clouds
287	Oct. 14	ER-2		(satellite, calibration south central United States)
288	Oct. 15		L, B	clear sky
290	Oct. 17	ER-2, Egrett, Twin Otter	L, B, R	clear sky
291	Oct. 18		L	clear sky
292	Oct. 19	ER-2, Egrett, Twin Otter	L, B, R	clear sky
294	Oct. 21	ER-2		(satellite calibration, south central United States)
295	Oct. 22	ER-2	B, R	clear sky
296	Oct. 23	ER-2		scattered clouds (transit across United States)
297	Oct. 24	Egrett, Twin Otter	L, B, R	thin cirrus
298	Oct. 25		L, B, R	scattered clouds
299	Oct. 26	Egrett, Twin Otter	L, B, R	solid cirrus deck; broken clouds
301	Oct. 28	Twin Otter	L, B, R	clear sky
303	Oct. 30	Egrett, Twin Otter	L, B, R	thick uniform stratus deck
304	Oct. 31		L, B, R	thick uniform stratus deck
305	Nov. 1	Egrett, Twin Otter	L, B, R	broken-to-solid stratocumulus

Ground station key: L, Lamont; B, Byron; R, Ringwood.

portant to follow the calibration procedures. The key to the operation of the RAMS radiometers is the comparison of the radiative signal incident on the detector, with an internally generated electrical signal synchronized 180° out of phase with the optical chopper. This signal is conducted through a resistive heating coating deposited on the detector surface. The resulting thermal signal is in opposition to that generated by the chopped optical radiation. The electrical signal is then adjusted by a microprocessor until a null is detected. At this point the electrically and radiatively generated signals are equal. The optical power absorbed by the detector is determined by calculating the electrical power required to produce a null output. Optical chopping helps to eliminate drift, and null balanced operation render the measurements insensitive to changes in detector responsivity, to amplifier gain, and to ambient temperature.

Because the detectors are absolute devices in the sense explained above, the calibration of the RAMS broadband radiometers is in reality a characterization of the optical front end of the instruments. The angular, power, and spectral response of the optical system are the fundamental elements of our calibration procedure.

The RAMS was calibrated before, during, and after the experiment. The calibration includes (1) power calibration, (2) angular response calibration, (3) spectral response calibration, and (4) surface and in-flight comparisons.

4.1. Power Calibration

The power calibration of the broadband radiometers was done using two different methods; (1) comparison with a Hickey-Frieden absolute cavity radiometer, and (2) high-altitude calibration from the ER-2 aircraft, flying at approximately 20 km altitude, using the Sun as a reference standard. The results of the calibrations using the cavity and high-altitude methods are compared in Table 2 for the two instruments that were utilized as reference instruments for the surface comparisons described in another section. It was found that the broadband power calibration coefficients obtained with methods 1 and 2 agree to better than 1% which is sufficient to meet the precision requirements of the experiment. The spectral differences between the broadband solar radiation at ER-2 altitude and at the surface are possibly partly responsible for the small differences noted. A correction for differences in spectral properties was not possible because a detailed spectral characterization of the cavity radiometer was not available. The broadband data were processed using the cavity radiometer calibrations validated by comparison with the high-altitude calibrated instruments.

The power calibrations of the TDDR were also done using two approaches; first, the National Institute of Standards (NIST) absolute lamp calibrations method and second, an ER-2 high-altitude calibration, similar to the one employed for the broadband instruments but using now the solar irradiance in each TDDR spectral channel. The NIST calibration values were used as preliminary; the high-altitude calibrations were used for the reduction of the TDDR data. In summary, the power calibration of the solar radiometers includes the following steps:

4.1.1. Cavity radiometer reference calibration at the surface. Before the field phase of the experiment, the broadband radiometers were compared with a Hickey-Frieden cavity radiometer, accurate to better than 1%, following the established method: point the cavity radiometer to the Sun under clear-sky

Table 2. RAMS Radiometer Calibration Constants

Detector	ER-2-Derived	Ground-Derived	Percent Difference
7A (TSBR)	3.28×10^6	3.26×10^6	0.6
18A (FSBR)	1.67×10^6	1.66×10^6	0.8

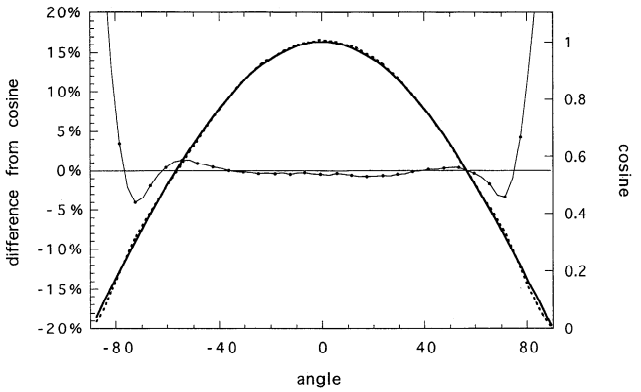

Figure 2. The angular response of a solar broadband radiometer is shown as a function of angle of incident light. The scale for the solid line (cosine function) and the dashed line (normalized detector signal) is on the right, while the scale for the symbols (percent deviation from cosine) is on the left.

conditions and then determine by comparison the radiometer calibration constant after subtracting the diffuse radiation field seen by the hemispherical field of view instruments and not seen by the relatively narrow field of view of the cavity radiometer (~5.5°). The diffuse field is determined by blocking the direct component of the solar flux using a shadow disk that blocks the hemispherical radiometer's field of view by an angle equal to the field of view of the cavity.

Errors in the reference total irradiance depend on the measurement of the diffuse flux which is measured as described above. Possible errors include the following:

1. Errors in calibration of the hemispherical field of view radiometer used to determine the diffuse radiation field are minimized using the same radiometer (the one under calibration) to determine total and diffuse fields. The diffuse field is determined by blocking the direct solar radiation with a shadow disc that covers an angle identical to the field of view of the reference cavity; the total flux is the measurement obtained with the shadow disc removed. From these measurements the fraction of the total flux corresponding to the direct radiation is obtained, and a calibration factor is deduced by comparison with the absolute cavity radiometer value.

2. Mismatching occurs between the blocking of the direct solar radiation and the 5.5° field of view of the cavity radiometer. The blocking disc size and distance from the radiometer's aperture require careful and accurate adjustment to properly match the field of view observed by the cavity instrument. Typical errors in this adjustment result in calibration errors of less than 0.2%.

3. Deviations from cosine response in the hemispherical radiometer render the diffuse field measurements sensitive to anisotropies in the observed scene (broken clouds, for example). The angular response of the radiometer is most critical in the evaluation of both the total and diffuse radiation fields. Accurate cosine response is key to accurate flux measurements. The angular response calibrations are discussed in section 5.2 below.

4.1.2. High-altitude, ER-2 calibration using the Sun as a reference. The high-altitude calibration that uses the solar constant as a reference was done during ARESE with data collected from the ER-2 aircraft. The radiometers were flown in the zenith-pointing position in the ER-2, and calibration factors were determined by comparing the known solar constant, after making the proper astronomical corrections, with the radiometer signal. Corrections for relative aircraft-Sun positions were made using data from the aircraft's navigational system and the algorithms described by *Hammer et al.* [1991]. A radiative transfer model (MODTRAN, including the standard stratospheric aerosol) is used to correct for atmospheric absorption and scattering above the ER-2 altitude. As many radiometers as possible were flown in the ER-2 zenith position by rotating them between the Egrett, Twin Otter, and ER-2 aircraft.

The high-altitude calibrations were utilized for the calibration of all radiometers, but it was most important for the calibration of the TDDR that requires calibrations under flight conditions, particularly due to the temperature sensitivity of the detectors. The TDDR channels could not be absolutely calibrated to better than about 5% because of the complicated angular response of their asymmetric optical system combined with uncertainties in the aircraft's navigational data. However, the precision of the ARESE TDDRs was about 1%.

4.2. Angular Calibration

The complex front end of the optical head of each radiometer is composed of reflective light collimating elements, diffuser, chopper, windows, and optical filters. These components are individually polished optical elements and have their own angular characteristics. High-quality radiometry demands the accurate knowledge of such angular response, not only as a quality control element but also as an important part of the calibration and data retrieval processes. Each instrument is calibrated for angular response in the laboratory by exposing the radiometers to a collimated radiation field and rotating the instrument in zenith and azimuth to obtain the angular response in a hemisphere. From our experience, optically symmetric radiometers (i.e., broadband radiometers) require only a zenith angular response calibration. Multiple channels instruments possessing azimuthal asymmetries (like the TDDR) require zenith and azimuth calibrations in each spectral channel.

Figure 2 shows the angular response of a solar broadband radiometer. The ordinate is the signal, and the abscissa is the angle of incidence of the collimated broad spectral band radiation. Note that the deviations from a perfect cosine response are within about ±2% up to almost 70°. The angular response varies from unit to unit, thereby the requirement for individual angular calibration of the radiometers. In many cases the deviations from perfect cosine response are within 1%. During the data processing the angular response calibrations are used, as described in the following section, to correct data to an ideal cosine response after estimating the direct and diffuse components of the flux.

Figure 3 depicts the angular calibration from a single channel of a Total Direct Diffuse Radiometer. The azimuth and zenith angular responses are combined in the figure. The z axis represents the angular response of the detector relative to an ideal cosine response. Just as with the broadband radiometers, the angular response calibrations are used to correct the data for cosine response.

The very accurate angular responses shown in Figures 2 and 3 eliminate the need for large corrections to be applied to the measured fluxes. However, in order to achieve the best possible results, we correct the measurements as follows.

4.2.1. Direct field correction. First, the ratio between direct and diffuse fluxes is estimated using the TDDR instrument

and/or model calculations (i.e., MODTRAN). The direct radiation flux is corrected by directly applying the angular response calibration values that correspond to the time varying angles of incidence determined from Sun position calculations (solar zenith and azimuth). The correction to the total flux is less than 1% for the angular response illustrated in Figure 2 and a total to diffuse ratio of 10.

Accurate measurements of the level of the radiometer optics are also required. This latter measurement is relatively simple for surface instruments. For aircraft the position of the radiometers relative to the Sun depends on the aircraft attitude, and the data are treated as described in a following section.

4.2.2. Diffuse field correction using the angular response function. The radiometer's angular response calibration is also used to correct the diffuse field. This is accomplished by first approximating the diffuse field as an isotropically emitting flat surface. Using this characterization, the radiation field is integrated over a hemispherical field of view, first using the measured angular response function and second, using an ideal cosine response. The ratio of these integrations yields the appropriate diffuse field correction which amounts to less than 0.2% for the angular response in Figure 2 and a total/diffuse ratio of 10.

4.3. Spectral Calibration

The filters employed in the broadband and spectral radiometers were calibrated for wavelength response by the manufacturer using normal spectroscopic techniques. This calibration, together with the power and angular calibrations, comprises the overall radiometer calibration. Figure 4 depicts the spectral band passes for the broadband radiometers and the center wavelength of the TDDR spectral channels (rectangular 10 nm full width at half maximum transmission).

4.4. Surface and In-Flight Comparison of Radiometers

4.4.1. Surface comparisons. The final step in our quality control and calibration procedures involves the comparison of all instruments with each other, by exposing them simultaneously to the open atmosphere radiation field. Comparisons at the surface are made for clear and cloudy atmospheres. This step is very useful in detecting errors and differences between instruments and to determine errors useful to estimate precision. If a large error is detected, the whole calibration process is traced back until the source is discovered and corrected.

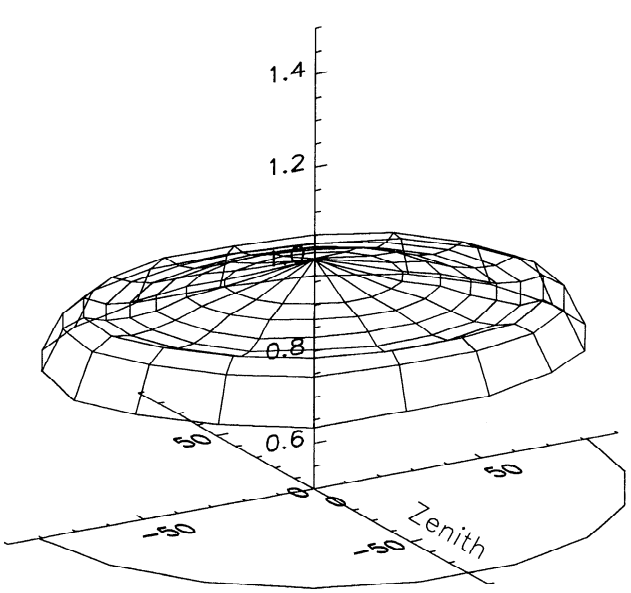

Figure 3. The azimuth and zenith angular responses are combined in this plot of the angular calibration of one of the total-direct-diffuse radiometer channels.

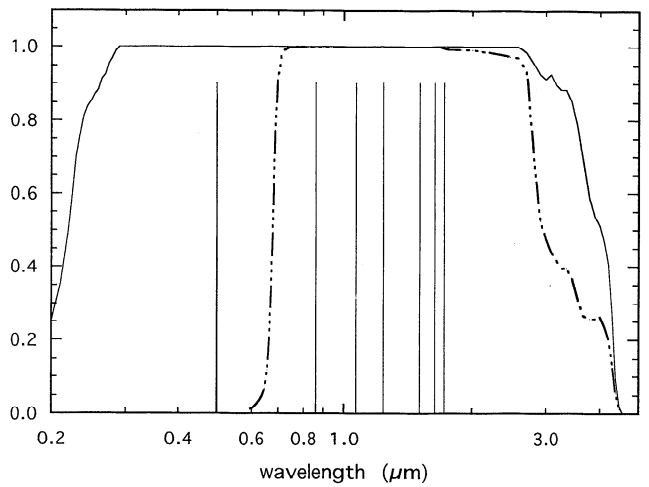

Figure 4. The spectral response curves are shown for the radiometers. The total solar broadband (solid line) has an effective square band pass of 0.224–3.91 μm, and the near-infrared broadband (dashed line) effective square band pass is 0.678–3.3 μm. Vertical lines indicate the center wavelengths of the seven narrowband channels of the total-direct-diffuse radiometer.

4.4.2. In-flight comparisons. On clear-sky days during ARESE, when it was logistically possible to fly the Egrett and Twin Otter aircraft at the same altitude and very close to each other "wing to wing," we compared the radiometric instrumentation for performance under actual flight conditions. A special flight plan was designed to help correct for offsets in the mounting of the instruments and in the aircraft's inertial navigational systems. The flight plan for instruments comparisons consisted of four data legs flown in directions directly toward and away from the Sun, as well as with the Sun perpendicular to the right and the left of the aircraft (Figure 5). The two former legs are useful to determine aircraft pitch offsets, and the two Sun perpendicular legs are useful to determine roll offsets.

Figure 6 depicts the radiometer comparison results after applying all aircraft navigational corrections and radiometric calibrations as discussed above. The average flux measurement is indicated for each instrument. Comparison of these values gives an idea of the precision of the instruments. Averaged values, tabulated in the figures, indicate excellent agreement. However, one particular case exhibiting large discrepancies should be noted. On October 17, 1995, the third comparison leg shows a discrepancy of about 70 W/m^2 between the Egrett and the Twin Otter zenith broadband radiometers. Such discrepancy is the result of the Egrett's tail partially shadowing the radiometer during the "away from the Sun" flight leg.

5. Airborne Measurements

The high-altitude Egrett was used as an above cloud platform flying in coordination with the low-altitude, below cloud, Twin Otter. The purpose of these aircraft was to provide si-

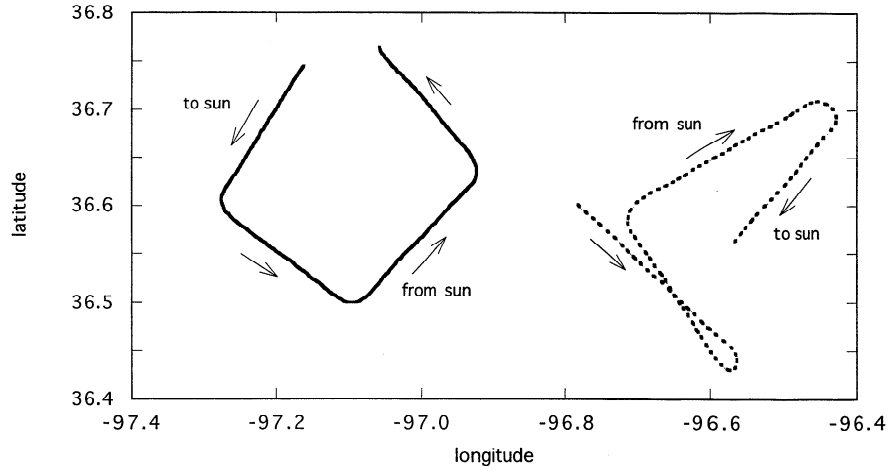

Figure 5. The solid curve in this plot is the track for the in-flight comparison of October 17, 1995. The dashed curve is the track for the October 19 in-flight comparison, displaced by 0.5 in longitude to simplify the plot. The straight segments are not exactly perpendicular or parallel due to changing solar azimuth.

multaneous and collocated measurements of net radiative fluxes at specified altitudes for a variety of conditions: cloudy, clear, and partly cloudy atmosphere. The Twin Otter top speed is below the Egrett's slowest operational speed. Such difference in speed was compensated for by periodically introducing 360° turns in the Egrett flight track (Figure 7). After each 360° turn, the Egrett was behind the Twin Otter and then proceeded past it, performing another data run. Data taken during turns and other maneuvers were eliminated from the data set.

The Egrett and Twin Otter aircraft were based at the Blackwell-Tonkawa airport, located 20 km to the northeast of the CART site. Data from the onboard instruments were telemetered to a receiving station located at the airport. The telemetry stream was recorded on tape in addition to being piped to a local computer network for real-time, in-flight monitoring. The Twin Otter carried an onboard tape recorder as backup. Data rates were 15.625 Hz for the Egrett and 12.5 Hz for the Twin Otter. During preflight operations on the ground the radiometers were covered so that the "dark" signals (offsets) could be measured. The aircraft typically took off at midmorning and flew in coordination for 2 to 5 hours. For the longer flights there was an interruption of about an hour while the Twin Otter returned to the airport and refueled. A total of 10 coordinated research flights were carried out by these airplanes.

The primary objectives of the ER-2 were to calibrate satellites and radiometers and to measure broadband and spectral reflectivity and net radiative fluxes for cloudy and clear skies at the tropopause. Throughout ARESE the ER-2 was based at Bergstrom Air Force Base in Austin, Texas. Fifteen ER-2 flights were carried out in support of this experiment. Eight

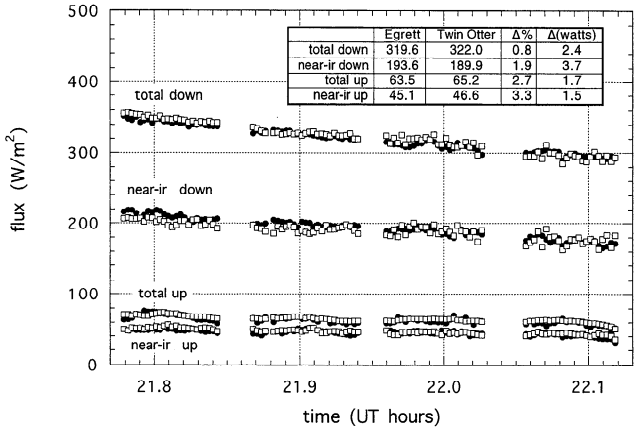

	Egrett	Twin Otter	Δ%	Δ(watts)
total down	319.6	322.0	0.8	2.4
near-ir down	193.6	189.9	1.9	3.7
total up	63.5	65.2	2.7	1.7
near-ir up	45.1	46.6	3.3	1.5

Figure 6. The two aircraft were flown side-by-side at the end of the October 26, 1995, flight in order to compare fluxes measured by the two sets of radiometers. The circles are Egrett values, and the open squares are Twin Otter values. Each symbol is a 10-s average, and overall average values are shown in the inset table. Each of the four "legs" of data span about 4–5 min in time and 15 km in distance. The sky was mostly clear during this time.

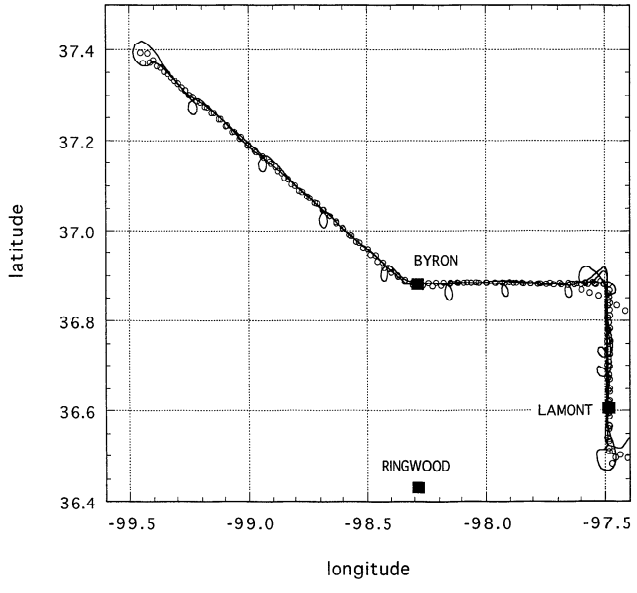

Figure 7. Flight tracks for the Egrett (solid line) and Twin Otter (open circles) are shown for October 24, 1995. The Twin Otter line is obscured by the Egrett line much of the time in this plot, illustrating the excellent coordination of the aircraft. The ground stations (squares) are also shown.

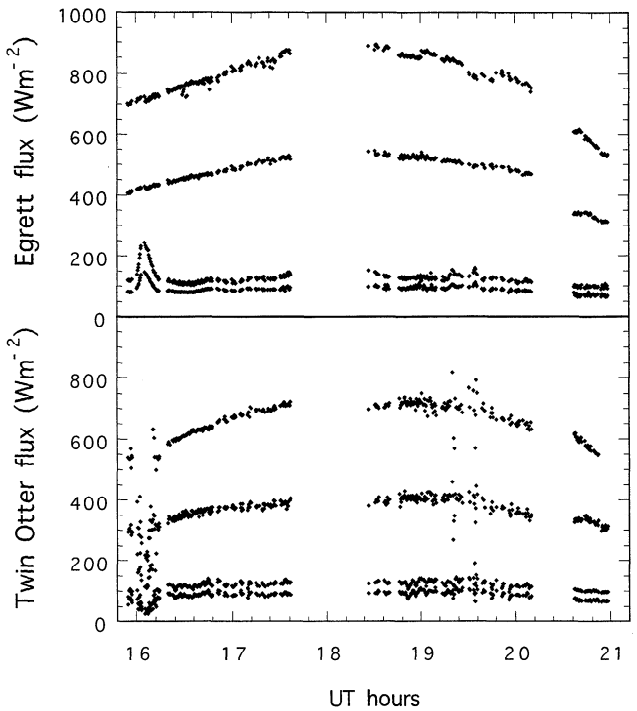

Figure 8. Data from the Egrett and Twin Otter broadband detectors are plotted as a function of UT hour for October 19, 1995. For each aircraft, in order of decreasing magnitude, are shown: downwelling solar flux, downwelling near-infrared flux, upwelling solar flux, and upwelling near-infrared flux. The gap around 1800 is when the Twin Otter went to refuel, and the gap around 2030 is when the aircraft were maneuvering to get into side-by-side (i.e., same altitude) formation. The effects of some broken clouds can be seen in the Twin Otter fluxes, particularly around 19 hours.

flights took place over the Oklahoma ground sites with six of the flights in coordination with the lower altitude aircraft. The ER-2, flying at a much higher speed in the stratosphere, but on the same ground track, flew over the other two aircraft numerous times during the coordinated missions. Four flights were dedicated to satellite calibration. As described above, all ER-2 flights during ARESE were also used to calibrate the zenith viewing radiometers using the Sun as a standard reference source.

6. Navigational Corrections

The data acquired from airborne platforms require corrections to determine the equivalent "horizontal platform" values of the measured irradiances. This is done following the method described by *Hammer et al.* [1991]. The basic problem is to position the Sun with coordinates fixed to the aircraft. This is achieved by transforming the vector representation of the Sun position in an Earth surface fixed coordinate system to an aircraft fixed coordinate system.

Once the data were reduced to a horizontal platform equivalent, the angular and other calibrations are applied, as described in a previous section. The navigational corrections are used to account for only fairly small deviations, less than 2° around the mean values in roll or pitch. The data acquired during airplane attitude exceeding the 2° limit were eliminated.

Figure 8 depicts an example of the irradiances measured on

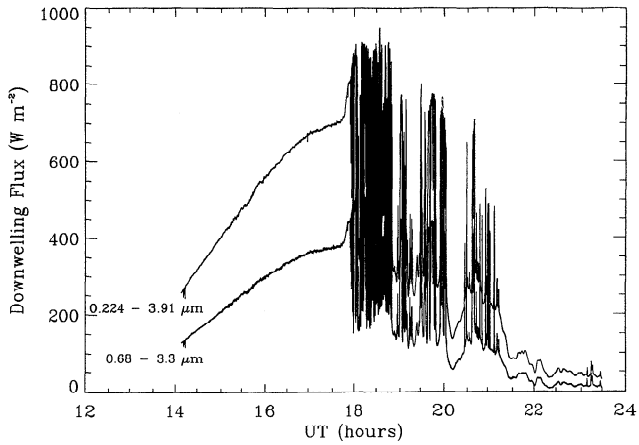

Figure 9. Broadband data from the CART site (Lamont) ground station are plotted as a function of UT hour for October 13, 1995.

October 19, 1995, by the Egrett and Twin Otter flying at 13.5 and 0.8–1.5 km altitude, respectively. The data during the period from 2030 to 2100 hours UT correspond to radiometer comparison legs that were flown at about 3.7 km altitude.

7. Surface Measurements

During ARESE, three ground stations acquired both broadband and spectral flux irradiances using instrumentation identical to that on the aircraft platforms with the exception of having only zenith pointing radiometers. The locations of these ground stations were determined by the preexisting network of ARM measurement facilities located in northern Oklahoma as well as by the planned flight trajectories of the aircraft involved in the ARESE, thereby providing measurements at the bottom of the atmospheric column examined in the stacked aircraft configuration. Additionally, being located at one of the ARM facilities provided supplemental information necessary for analysis of the data (i.e., ozone and standard sondes, various meteorological readings, LIDAR and RADAR measurements, etc.). Additionally, Baseline Solar Radiation Network (BSRN) measurements and Solar and InfraRed Observation Stations (SIROS) measurements are available for comparison and cross reference. A comparison of the RAMS, BSRN, and SIROS is discussed by *Bush et al.* [1997] and *Bush and Valero* [1997].

The three surface stations were located at the central CART facility in Lamont and at the Byron and Ringwood extended facilities along the northern and southern ARESE flight tracks (Figure 7). The data acquisition system was located below the three radiometer mounting boxes in a tent to protect it from the natural elements. The stations were operated during all Oklahoma based aircraft missions between October 11 and November 1, 1995, as well as on several selected nonflight days to supplement the overall data set. Typical operation times spanned sunrise to sunset, minus a few hours on either end. Standard operating procedures included a brief (30 min) period for instrument warm-up as well as "dark" signal baseline determinations. All calibrations were completed prior to deployment of the instruments to the field and verified after the experiment.

Data were acquired at a nominal rate of 10 Hz which was more than adequate for the broadband instruments but necessary for the TDDR in resolving features associated with its

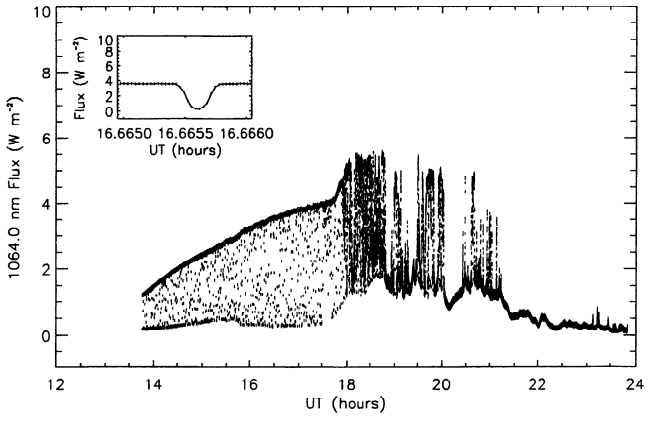

Figure 10. Data from the 1064 nm channel of the total-direct-diffuse radiometer are plotted for the same interval as the previous figure. The inset shows a small region of the data to illustrate the effect of the shadow ring.

shadow ring. Figures 9 and 10 depict samples of the broadband and TDDR data acquired at the Lamont (CART central facility site) Ground Station on October 13, 1995. During this date, atmospheric conditions changed from clear to broken clouds to heavy overcast.

The upper and lower curves in Figure 9 show hemispherical downwelling irradiance for the band passes 0.224–3.91 and 0.678–3.3 μm, respectively. The visible portion of the spectrum (0.224–0.678 μm) is calculated as the difference between these two signals. Effects of scattering off the edges of clouds are seen from 1800 to 2130 hours UT when a broken cloud field prevailed. After 2130, overcast conditions predominated.

In Figure 10 one of the seven TDDR spectral channels (1064 nm) is displayed. The effect of the shadow ring can be seen in this figure, particularly during the clear atmosphere period. The maximum envelope of this graph represents the variation of the total hemispherical downwelling flux, whereas the minimum envelope is essentially the variation of the diffuse portion of this flux. The resulting difference of these two components is thus a measurement of the direct solar signal. The direct component of the flux may then be used to calculate optical depths of the atmospheric column. The inset of this figure expands a small region of the TDDR data showing the amount of data needed to resolve a single dip during a shadow ring transit. Without a large enough data rate the dip may not be adequately resolved, and thus the direct and diffuse components, and any information derived from them, could not be accurately determined.

8. Discussion

The general strategy followed during ARESE was briefly discussed with the objective to inform potential users of the data which is freely available at the ARM ARESE data archive via anonymous FTP to ftp.arm.gov.

The radiometric data introduced in this paper provides information necessary to assess the magnitude and overall spectral distribution of the excess absorption of solar radiation by clouds and of the absorption by the clear atmosphere. A major consideration in the planning of the experimental strategy for ARESE was related to the sampling issues discussed by *Ackerman and Cox* [1981].

An important difference between our calibration methods and others is the introduction of the angular response calibrations, not just as a quality control procedure but as a necessary practice in high-quality radiometry. The final retrieved irradiances incorporate corrections applied on the basis of the angular calibration of each instrument.

The power calibration of the broadband radiometers is validated against the solar constant using the ER-2 high-altitude observations. It is most important, for purposes of model-measurements comparisons and satellite calibration, that the radiometer measurements and models be referenced to the same standard (the solar constant). High-altitude ER-2 calibrations are employed for the narrow spectral band pass channels of the TDDR.

The in-flight "wing to wing" comparisons illustrated in Figure 6 validate the precision of the data in real flight conditions. Analyses of the data presented here are reported by *Zender et al.* [this issue] and *Valero et al.* [this issue].

Acknowledgments. The authors gratefully acknowledge the Department of Energy's ARM program and its Unmanned Aerospace Vehicle (ARM-UAV) component, the Strategic Environmental Research and Development Program (SERDP) of the Department of Defense, and NASA. This work was also supported by the Department of Energy through grant DEFG0395ER69183 to the Scripps Institution of Oceanography, and contracts 351574-AQ5 and 352731-AQ5 with Batelle Memorial Institute, Pacific Northwest National Laboratories.

References

Ackerman, S. A., and S. K. Cox, Aircraft observations of shortwave fractional absorptance of non-homogeneous clouds, *J. Appl. Meteorol.*, *20*, 1510–1515, 1981.

Ackerman, A. S., and O. B. Toon, Unrealistic desiccation of marine stratocumulus clouds by enhanced solar absorption, *Nature*, *380*, 512–515, 1996.

Arking, A., Absorption of solar energy in the atmosphere: Discrepancy between models and observations, *Science*, *273*, 779–782, 1996.

Bush, B. C., and F. P. J. Valero, Comparison of ARESE clear sky surface radiation measurements, *J. Quant. Spectrosc. Radiat. Transfer*, in press, 1997.

Bush, B. C., S. K. Pope, A. Bucholtz, F. P. J. Valero, and A. Strawa, Surface radiation measurements during the ARESE campaign, *J. Quant. Spectrosc. Radiat. Transfer*, in press, 1997.

Cess, R. D., et al., Absorption of solar radiation by clouds: Observations versus models, *Science*, *267*, 496–499, 1995.

Chou, M. D., and W. D. Zhou, Estimation and model validation of the surface solar radiation and cloud radiative forcing using TOGA COARE measurements, *J. Clim.*, *10*(N4), 610–620, 1997.

Francis, P. N., J. P. Taylor, P. Hignett, and A. Slingo, On the question of enhanced absorption of solar radiation by clouds, *Q. J. R. Meteorol. Soc.*, *123*, 419–434, 1997.

Geist, J., and W. R. Blevin, *Appl. Opt.*, *12*, 2532, 1973.

Hammer, P. D., F. P. J. Valero, and S. Kinne, The 27–28 October 1986 FIRE cirrus case study: Retrieval of cloud particle sizes and optical depths from comparative analyses of aircraft and satellite-based infrared measurements, *Mon. Weather Rev.*, *119*, 1673–1692, 1991.

Imre, D. G., E. H. Abramson, and P. H. Daum, Quantifying cloud-induced shortwave absorption: An examination of uncertainties and of recent arguments for large excess absorption, *J. Appl. Meteorol.*, *35*, 1991–2010, 1996.

Kiehl, J. T., and K. E. Tremberth, Earth's annual global mean energy budget, *Bull. Am. Meteorol. Soc.*, *78*(N2), 197–208, 1997.

King, M. D., L. F. Radke, and P. V. Hobbs, Determination of spectral absorption of solar radiation by marine stratocumulus clouds from airborne measurements within clouds, *J. Atmos. Sci.*, *47*, 894–907, 1990.

King, M. D., et al., Airborne scattering spectrometer for remote sensing of cloud, aerosol, water vapor, and surface properties, *J. Atmos. Oceanic Technol.*, *13*, 777–794, 1996.

Kondratiev, K. Y., V. I. Binenko, and I. N. Melnikova, Solar radiation absorption by cloudy and cloudless atmospheres, *Meteorol. Gidrol.*, *N2*, 14–23, 1996.

Li, Z., and L. Moreau, Alteration of atmospheric solar absorption by clouds: Simulation and observation, *J. Appl. Meteorol.*, *35*, 653–670, 1996.

Li, Z., H. W. Barker, and L. Moreau, The variable effect of clouds on atmospheric absorption of solar radiation, *Nature*, *376*, 486–490, 1995.

Pilewskie, P., and F. P. J. Valero, Direct observations of excess solar absorption by clouds, *Science*, *267*, 1626–1629, 1995.

Ramanathan, V., et al., Warm pool heat budget and shortwave cloud forcing: A missing physics?, *Science*, *267*, 499–503, 1995.

Spinhirne, J. D., W. D. Hart, and D. L. Hlavka, *J. Atmos. Sci.*, *53*, 1438, 1996.

Stephens, G. L., How much solar radiation do clouds absorb?, *Science*, *271*, 1131–1133, 1996.

Stephens, G. L., and S. C. Tsay, On the cloud absorption anomaly, *Q. J. R. Meteorol. Soc.*, *116*, 671–704, 1990.

Valero, F. P. J., W. J. Y. Gore, and L. P. M. Giver, Radiative flux measurements in the troposphere, *Appl. Opt.*, *21*, 831–838, 1982.

Valero, F. P. J., R. D. Cess, M. Zhang, S. K. Pope, A. Bucholtz, B. Bush, and J. Vitko, Absorption of solar radiation by the cloudy atmosphere: Interpretations of collocated aircraft measurements, *J. Geophys. Res.*, this issue.

Waliser, D. E., W. D. Collins, and S. P. Anderson, An estimate of the surface shortwave cloud forcing over the western Pacific during TOGA COARE, *Geophys. Res. Lett.*, *23*, 519–522, 1996.

Zender, C. S., S. K. Pope, B. Bush, A. Bucholtz, W. D. Collins, J. T. Kiehl, F. P. J. Valero, and J. Vitko, Atmospheric absorption during the Atmospheric Radiation Measurements Enhanced Shortwave Experiment (ARESE), *J. Geophys. Res.*, this issue.

A. Bucholtz, B. C. Bush, P. Flatau, S. K. Pope, and F. P. J. Valero, Atmospheric Research Laboratory, Center for Atmospheric Sciences, Scripps Institution of Oceanography, University of California, San Diego, La Jolla, CA 92093-0242. (e-mail: abucholtz@ucsd.edu; brbush@ucsd.edu; pflatau@ucsd.edu; spope@ucsd.edu; fvalero@ucsd.edu)

W. D. Collins, National Center for Atmospheric Research, 1850 Table Mesa Drive, Boulder, CO 80303. (e-mail: wcollins@kavieng.cgd.ucar.edu)

W. J. Y. Gore and A. Strawa, NASA Ames Research Center, Moffett Field, CA 94035. (e-mail: strawa@ra.arc.nasa.gov)

(Received March 20, 1997; revised August 7, 1997; accepted August 26, 1997.)